Journal of Magnetic Resonance Open 20 (2024) 100152

Contents lists available at ScienceDirect

Journal of Magnetic Resonance Open

journal homepage: www.sciencedirect.com/journal/journal-of-magnetic-resonance-open

Research Article

Biradicals based on PROXYL containing building blocks for efficient dynamic nuclear polarization in biotolerant media

Kevin Herr [a], Mark V. Höfler [a], Henrike Heise [b,c], Fabien Aussenac [d], Felix Kornemann [a], David Rosenberger [e], Martin Brodrecht [a], Marcos de Oliveira Jr. [f], Gerd Buntkowsky [a,*], Torsten Gutmann [a,*]

[a] Institute of Physical Chemistry, Technical University Darmstadt, Peter-Grünberg-Straße 8, D-64287, Darmstadt, Germany
[b] Institute of Biological Information Processing, Structural Biochemistry (IBI-7), Forschungszentrum Jülich, D-52425, Jülich, Germany
[c] Institut für Physikalische Biologie, Heinrich-Heine-Universität Düsseldorf, D-40225, Düsseldorf, Germany
[d] Bruker France SAS, 34 rue de l'industrie, F-67160, Wissembourg, France
[e] Institute of Physics, Free University Berlin, Arnimallee 12, D-14195, Berlin, Germany
[f] São Carlos Institute of Physics, University of São Paulo, PO Box 369, 13560-970, São Carlos, SP, Brazil

ARTICLE INFO

Keywords:
Biradicals
Peptides
Spin labeling
Solid-state nmr
Dynamic nuclear polarization

ABSTRACT

A versatile strategy for synthesizing tailored peptide based biradicals is presented. By labeling the protected amino acid hydroxyproline with PROXYL via the OH functionality and using this building block in solid phase peptide synthesis (SPPS), the obtained peptides become polarization agents for DNP enhanced solid-state NMR in biotolerant media. To analyze the effect of the radical position on the enhancement factor, three different biradicals are synthesized. The PROXYL spin-label is inserted in a collagen inspired artificial peptide sequence by binding through the OH group of the hydroxyproline moieties at specific position in the chain. This labeling strategy is universally applicable for any hydroxyproline position in a peptide sequence since solid-phase peptide synthesis is used to insert the building block. High performance liquid chromatography (HPLC) and mass spectrometry (MS) analyses show the successful introduction of the spin label in the peptide chain and electron paramagnetic resonance (EPR) spectroscopy confirms its activity. Dynamic nuclear polarization (DNP) enhanced solid-state nuclear magnetic resonance (NMR) experiments performed on frozen aqueous glycerol-d_8 solutions containing these peptide radicals show significantly higher enhancement factors of up to 45 in $^{1}H \rightarrow ^{13}C$ cross polarization magic angle spinning (CP MAS) experiments compared to an analogous mono-radical peptide including this building block ($\varepsilon \approx 14$). Compared to commercial biradicals such as AMUPol for which enhancement factors > 100 have been obtained in the past and which have been optimized in their structure, the obtained enhancement up to 45 for our biradicals presents a significant progress in radical design.

Introduction

Nuclear magnetic resonance (NMR) is a versatile spectroscopic technique that enables the structural characterization of biomolecules at an atomic level. It provides information on the constitution and assembly of these molecules, and sheds light on local environments even in complex solid or soft matter materials. However, this technique suffers from its low intrinsic sensitivity. To overcome this issue, solid-state dynamic nuclear polarization (DNP) enhanced NMR at high magnetic field has become popular in the last years [1-14]. This technique uses the three order of magnitude higher polarization of electron spins -and transfers it into nuclear spin polarization by appropriate mechanisms [15,16]. In the most common type of experiment, the sample for analysis is dissolved in an aqueous or an organic solvent together with an electron spin source such as a biradical. The experiment is then performed either on the frozen sample, typically at about 110 K (solid-state DNP) or after rapid thawing of the sample (dissolution DNP).

Conventional biradicals, optimized for very high DNP enhancement factors, are often expensive and large efforts have been made in the past to synthesize and systematically characterize them [17-23]. Only few of them are soluble in aqueous media [24-31] and thus many of them require solubility mediators [20,32,33]. Efficient biradicals for DNP

* Corresponding authors.
E-mail addresses: gerd.buntkowsky@chemie.tu-darmstadt.de (G. Buntkowsky), gutmann@chemie.tu-darmstadt.de (T. Gutmann).

https://doi.org/10.1016/j.jmro.2024.100152

Available online 31 May 2024

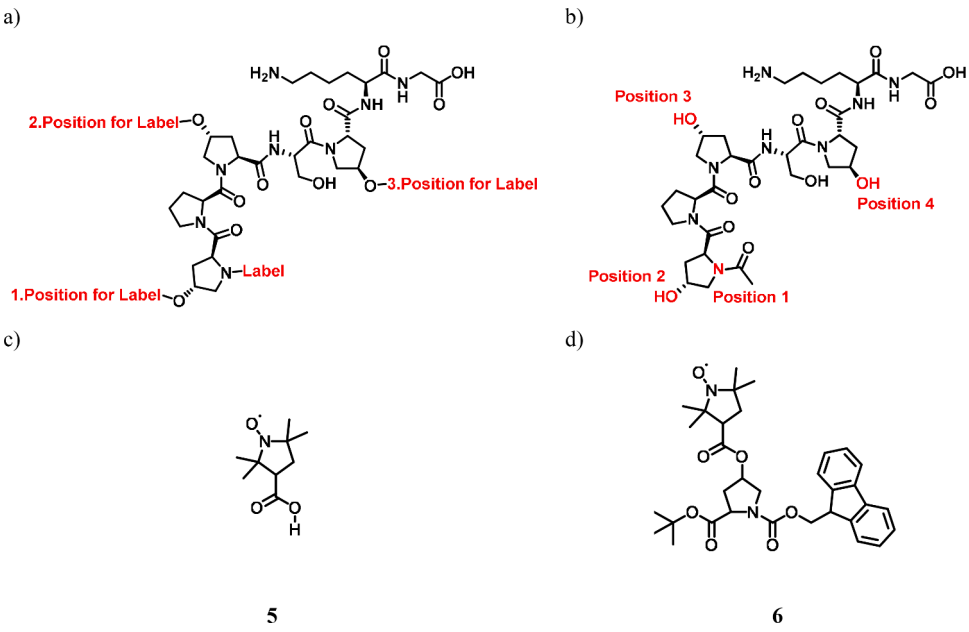

Fig. 1. Upper panel: a) Illustration of the model peptide sequence NH—Hyp-Pro-Hyp-Ser-Hyp-Lys-Gly-OH. The possible label positions (the three positions of the hydroxyprolines 2–4 and the N-terminus 1) are marked in red. b) Illustration of the peptide sequence Acetyl-Pro-Pro-Pro-Ser-Pro-Lys-Gly-OH used for the molecular dynamic simulations. Red atoms represent the four possible functionalization positions. **Lower panel:** Structures of c) 3-Carboxy-PROXYL **5** and d) Fmoc-*NH*—Hyp (OOC-PROXYL)-O^{t}Bu **6**.

applications need to be synthesized in challenging multiple step syntheses as rigid systems with a certain geometry and distance between the radical centers [20,34-37]. To provide novel biradicals with a minimized cost and synthetic effort, peptides may be utilized that include radical containing building blocks. Specifically designed spin-labeled peptides are suitable for in-cell or lipid membrane studies as shown by Sani and co-workers employing single and double TOAC labeling [38,39]. In their studies, they achieved ^{13}C signal enhancements of up to 13 and 25 for peptide mono-radicals and biradicals, respectively, at 9.4 T and nominally 110 K. In parallel, some of the authors have introduced a PROXYL containing building block to an artificial peptide. For this peptide mono-radical, they obtained an enhancement of 14 in ^{13}C MAS DNP experiments under similar conditions (9.4 T and nominally 110 K) [40].

To prepare biradical-peptides with PROXYL containing building blocks, a rigid peptide sequence derived from collagen can be used, which is an important component of structure proteins present in teeth, bones and tissues. It consists of several hydroxyproline moieties. The cyclic structure of the amino acid hydroxyproline leads to a reduced number of degrees of freedom, while the reactive OH group of the hydroxyproline allows its modification with a radical spin label such as PROXYL.

In this work, we employ the collagen-based peptide NH—Hyp-Pro-Hyp-Ser-Hyp-Lys-Gly-OH (Fig. 1), as model compound to demonstrate the site-directed DNP spin-labeling of polypeptides. There are four possible spin-labeling positions in the peptide (Fig. 1a), namely the three hydroxyprolines (2–4) and the N-terminus (1). By combining different positions, it is possible to achieve biradicals with various electron-electron distances.

Three different biradical-peptides (Fig. 1) are synthesized, purified by high performance liquid chromatography (HPLC) and characterized by mass spectroscopy. The radical activity of the spin labels is tested by electron paramagnetic resonance (EPR) spectroscopy. As a highlight the novel radical spin labels are applied in solid-state DNP NMR experiments in frozen aqueous solution to demonstrate their efficiency to boost sensitivity.

Experimental section

Synthetic protocols

Detailed synthetic protocols and sample characterizations are given in the appendix.

Electron paramagnetic resonance (EPR)

The EPR spectra for all samples were measured on an X-band EPR Miniscope MS-400 (Magnettech, Germany) equipped with an A TC H03 temperature controller and a rectangular TE102 resonator operating at 9.43 GHz. All EPR spectra were recorded with a modulation amplitude of 0.1 mT and a modulation frequency of 100 kHz. Spectra were taken under 24 dB of microwave attenuation with a mantissa gain of 1 and an exponential gain of 1. Measurements were performed at 298 K and at 100 K. A magnetic field range of 14 mT was swept with a center B_0 field of 337 mT with a sweeping time of 60 s to acquire 2048 points.

Spectral simulations were performed using the software package EasySpin [41], implemented in Matlab®. Room temperature spectra were simulated according to two models: (Model 1) single radicals experiencing isotropic Brownian motion in the fast regime, modeled by the solutions of the Stochastic Liouville equation, as implemented in the function *chili* of EasySpin [41]; (Model 2) a biradical experiencing chemical exchange between two configurations with a variable exchange rate. The first chemical configuration is represented by a two-electron system with electron-electron spin exchange interaction parameter (J) with much larger magnitude than the isotropic hyperfine interaction parameter (A_{iso}), $|J| >> |A_{iso}|$, while the second configuration is represented by a system with two non-interacting electrons, $|J| << |A_{iso}|$. Model 2 simulations were performed using the EasySpin add on function *exchange* [41,42]. Frozen solution spectra were simulated using the function *pepper*, implemented in EasySpin [41].

DNP enhanced solid-state NMR experiments

All spectra were measured at a Bruker Avance III 400 DNP spectrometer with an operating field of 9.4 T which corresponds to a

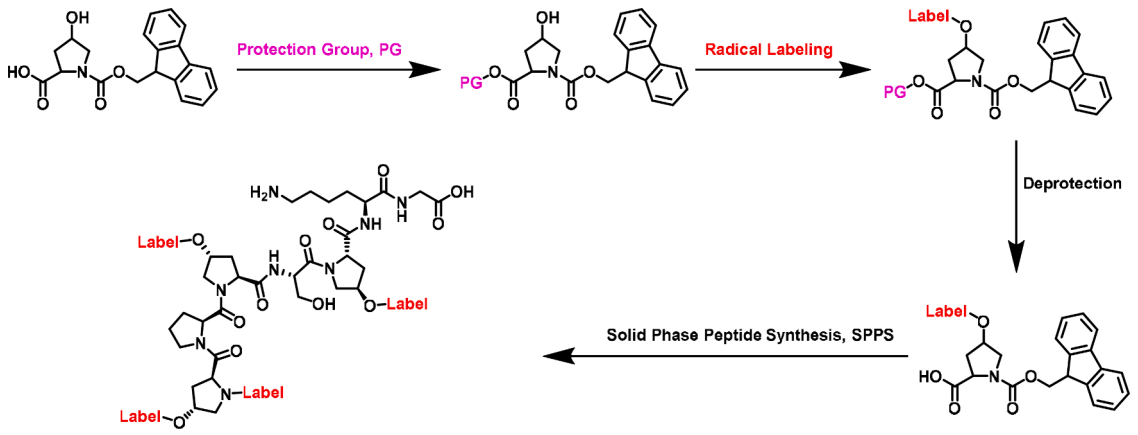

Scheme 1. Synthesis strategy for labeling Fmoc-hydroxyproline with the radical and implementing it into a SPPS protocol. The obtained collagen inspired sequence NH—Hyp-Pro-Hyp-Ser-Hyp-Lys-Gly-OH delivers three possible positions for the labeled amino acid and one more for the label itself at the N-terminus. Note: The synthesis of the radical labeled building block is adapted from ref. [40] where its basic DNP activity has been tested in a peptide mono-radical.

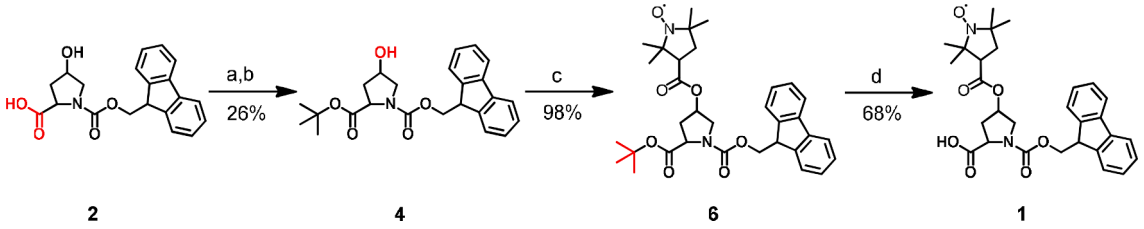

Scheme 2. Synthesis of the radical labeled Fmoc-hydroxyproline **1.** a) Diisopropylcarbodiimide, copper(I)-chloride, tert-butanol, RT, 14 h; b) THF, 0 °C, 18 h; c) 3-Carboxy-PROXYL **5**, EDC•HCl, DMAP, RT, 12 h; d) TFA, RT, 1,5 h. The presented reaction scheme to prepare **1** is adapted from ref [40]. where the synthesis of this building block has been described and its basic DNP activity tested in a peptide mono-radical. The yields are given for each single synthesis step in percent. Taking these values an overall yield of the building block **1** of 17 % is obtained.

frequency of 401.63 MHz for ^{1}H and 100.99 MHz for ^{13}C. The spectrometer was equipped with a 3.2 mm low temperature H/X/Y triple resonance probe operating in ^{1}H/^{13}C/^{15}N mode. Microwaves with a frequency of 263 GHz were generated by a 9.7 T Bruker gyrotron system. All spectra were recorded with a spinning rate of 8 kHz.

Firstly, the ^{1}H build-up times T_B of the samples were measured. For this, a saturation recovery pulse sequence was used with a saturation pulse train of twenty $\pi/2$ pulses with a pulse length of 2.3 µs for ^{1}H and a pulse spacing of 200 µs. The analysis of the build-up time was performed with the Bruker topspin software applying an exponential fit function (ESI Figures S21-S23). The resulting build-up times were 2.9 s, 1.8 s and 4.2 s for the peptides **7, 8** and **9**, respectively.

^{1}H MAS spectra were recorded with a modified background suppression pulse sequence derived from the Bruker zgbs sequence [43]. For excitation, a $\pi/2$ pulse with a length of 2.3 µs was used. Each spectrum was measured with 16 scans and a recycle delay of $1.3*T_B$.

^{1}H→^{13}C CP MAS spectra were recorded with a contact time of 2 ms with a linear 100–50 ramp on ^{1}H and a recycle delay of $1.3*T_B$. An acquisition time of 30 ms was employed and heteronuclear spinal 64 [44] decoupling applied during data acquisition. Each spectrum was recorded with 128 scans and referenced to the signal of the silicon plug (-Si-$\underline{C}H_3$, 0 ppm).

Results and discussion

Synthesis of the spin labeled Fmoc amino acid

There are two general synthesis strategies, which can be used to label

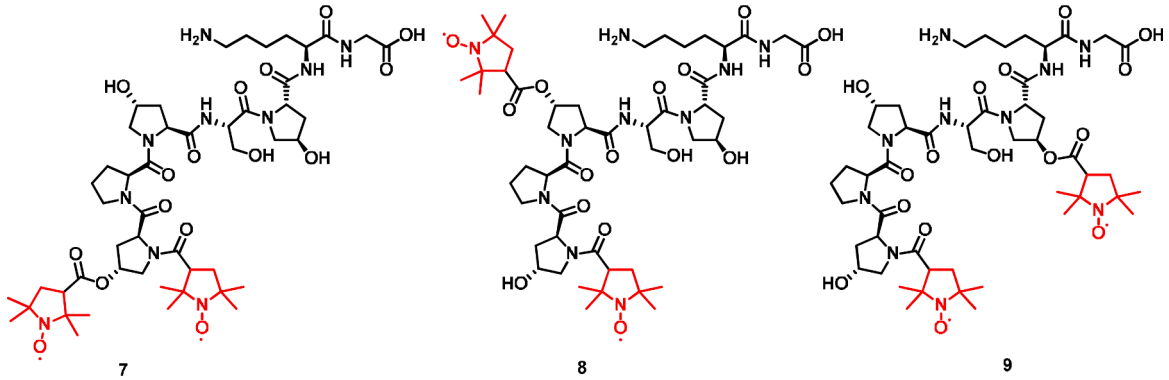

Fig. 2. Synthesized peptide based biradicals **7–9** with different distances between the radical centers. All structures are based on the NH—Hyp-Pro-Hyp-Ser-Hyp-Lys-Gly-OH sequence.

the NH—Hyp-Pro-Hyp-Ser-Hyp-Lys-Gly-OH peptide sequence, the top-down and the bottom-up principle. Post synthetic approaches per top-down principle such as click-chemistry with azide-alkyne or maleimide coupling are well known but have the downside of requiring special functional precursors [45-53]. These precursors are often expensive or commercially not available.

For this reason, we explore in this work the bottom-up principle to create novel peptide based biradicals by insertion of the radical during solid phase synthesis. This approach is illustrated in Scheme 1.

Here, a pre-synthesized radical labeled Fmoc-hydroxyproline is used in the solid phase peptide synthesis (SPPS) [54,55] protocol.

Scheme 2 shows the general synthesis strategy for the radical labeled Fmoc-hydroxyproline **1** as used also in our previous work [40]. It follows a Steglich esterification reaction [56] after protecting selectively the free carboxyl group of the C-terminus of the Fmoc-hydroxyproline **2**. The necessary protection agent O-tert-butyl-N,N'-diisopropylisourea **3** has been synthesized similar to Huerta et al. [57] by using a copper(I) catalyst, activating *tert*-butanol with diisopropylcarbodiimide. This agent is used for the selective protection of the C-terminus of Fmoc-hydroxyproline yielding **4**. After purification by column chromatography, it is feasible to couple the radical 3-carboxy-PROXYL **5** to the amino acid building block by using the reactive hydroxyl group of its side chains for an esterification reaction. The resulting radical compound **6** is obtained with 98 % yield. After the deprotection of the carboxyl group is performed by acidolysis and the final purification by column chromatography, the radical labeled Fmoc-hydroxyproline **1** is obtained with 68 % yield.

Having successfully isolated the target compound **1** and validated it by HPLC, MS and EPR (see ESI and experimental section), it is introduced into the SPPS to receive an artificial peptide sequence with rigid structure containing radical labels at specific positions.

In addition, the N-terminus of the peptide is labeled with the radical 3-carboxy-PROXYL **5**. In this way, the three biradicals **7, 8** and **9** shown in Fig. 2 containing different geometries and distances of the radical centers have been synthesized via SPPS. The as-obtained sequences have been validated by HPLC and MS (see ESI and experimental section).

Estimation of rigidity by molecular dynamic simulations

As shown in previous studies the achievable signal amplification of biradicals in DNP experiments strongly depends on the geometry and distance between the radical centers as well as on the rigidity of their structure [58]. To estimate the rigidity of the backbone scaffold of our novel peptide biradicals, molecular dynamics (MD) and replica exchange molecular dynamics (REMD) simulations of the simplified heptapeptide model sequence NH-Pro-Pro-Pro-Ser-Pro-Lys-Gly-OH were performed. In this sequence the original hydroxyproline residues are replaced by proline. This simplification does not significantly influence the structure and stiffness of the overall molecule as it has been shown in previous studies [59,60], and enables us to employ the predefined CHARMM27-force-field implemented in the GROMACS 2019 v2 software [61]. The simulations reveal a high stiffness, visible by the small distance errors, of the backbone scaffold shown in Fig. 1b with a N—N distance from proline-1 to proline-4 of 1.14 ± 0.11 nm (MD) and 1.13 ± 0.11 nm (REMD), respectively. Details on distance distributions calculated for the model peptide are given in the ESI Figure S24 and Table S2. Finally, from the root mean squared deviation (RMSD) with respect to the initial peptide configuration as a function of time for all peptide atoms and the $C_\alpha$atoms (ESI Table S3) it is clearly visible that the atoms move no further than 0.20 (±0.08) nm away from their initial position during the MD simulations. This underlines the high rigidity of the peptide structure, which is further emphasized by the very small standard deviations. The overall dimensions of the oligopeptide are also very rigid as shown by the small fluctuations in R_g and R_{end} in ESI Table S3.

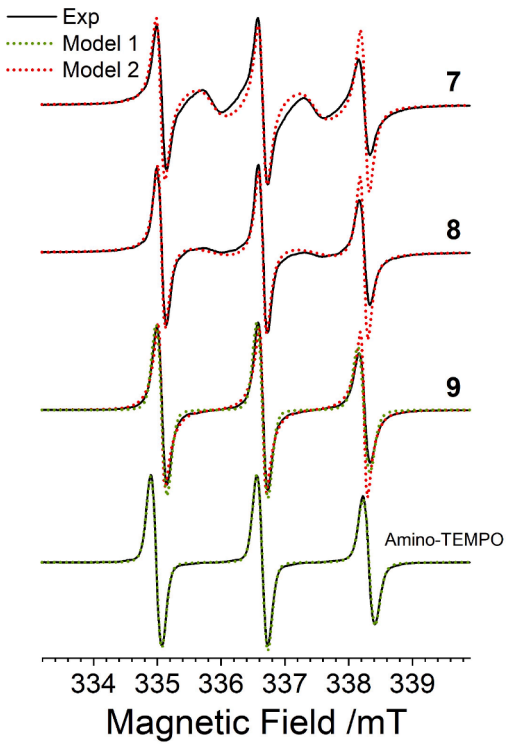

Fig. 3. EPR spectra of ca. 15 mM of **7, 8, 9** and amino-TEMPO as reference in a glycerol-d_8/D_2O/H_2O (60/30/10) at 298 K. Simulated spectra are also shown for two different models. Model 1 considers an isolated nitroxide radical in solution experiencing isotropic Brownian motion with correlation times of 0.1 and 0.2 ns for amino-TEMPO and **9** respectively. Model 2 assumes a biradical system with two ^{14}N nuclei in solution experiencing chemical exchange between two configurations with different exchange rate constants (see main text) [42]. The model assumes the presence of solely two conformations: one characterized by |J| significantly greater than |A|, and another with |J| significantly smaller than |A|. In the former scenario, a coupled spin-1 system interacts with two ^{14}N nuclei, while in the latter, two distinct spin-1/2 systems each interact with a single ^{14}N nucleus. The high-field line intensities are not well reproduced by Model 2 because stochastic motion in the liquid is not taken in account by the simulation method.

Proof of spin label activity

The chemical integrity of the radical centers in the synthesized peptide based biradicals **7, 8** and **9** has to be validated by qualitative EPR to guarantee the feasibility to use them in DNP experiments. Fig. 3 shows the EPR spectra for biradicals **7, 8** and **9**, and for the amino-TEMPO mono-radical as a reference. The samples are dissolved in a glycerol-d_8/D_2O/H_2O (60/30/10) biotolerant matrix and measured at 298 K at a concentration of 15 mM. All three biradical peptides show EPR-activity which confirms that significant amounts of the nitroxyl spin labels are still active after all reaction steps of the SPPS. The EPR lineshapes are dominated by the hyperfine coupling interaction with ^{14}N, giving the well documented triplet in liquid state [62]. The spectrum of the amino-TEMPO mono-radical can be simulated (Model 1 in Fig. 3) assuming a single nitroxide radical experiencing isotropic Brownian motion, modeled by the solutions of the Stochastic Liouville equation. Simulation parameters are: axial hyperfine coupling with ^{14}N with principal values $A_{\parallel} = 108.6$ MHz and $A_{\perp} = 15.9$ MHz (A_{iso}= 46.8 MHz), *g*-tensor principal values $g_{xx} = 2.0069$, $g_{yy} = 2.0051$, $g_{zz} = 2.0009$ (g_{iso}= 2.0043) and a correlation time for the isotropic motion of 0.1 ns.

For samples **7–9** single electron simulations do not reproduce well the observed lineshapes. As an example, the spectrum of **9** was simulated using the same model applied for amine-TEMPO (Model 1). The simulation reproduces well the peak intensities with correlation times for

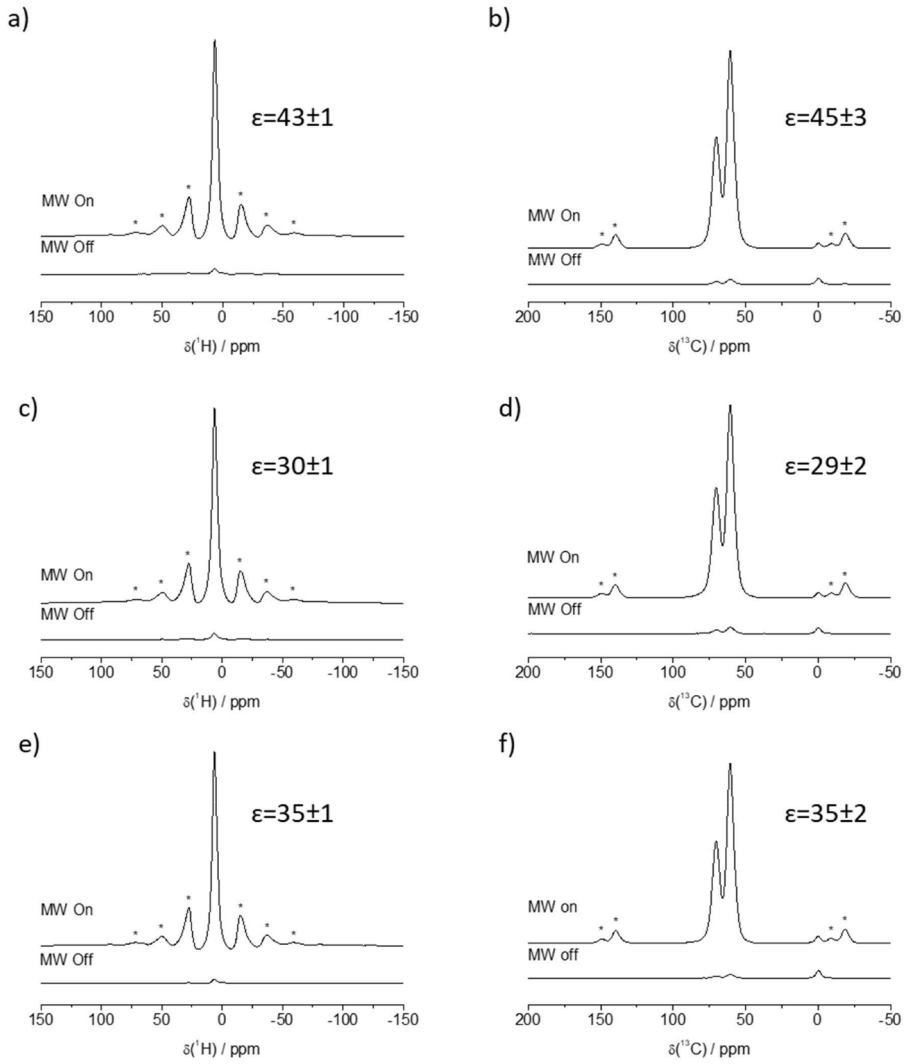

Fig. 4. DNP enhanced ^{1}H MAS (a,c,e) and ^{1}H→^{13}C CP MAS NMR (b,d,f) spectra of 15 mM peptide based biradical (a,b) **7**, (c,d) **8** and (e,f) **9** in glycerol-d_8/D_2O/H_2O (60/30/10). Note: Spectra were measured at 9.4 T at a spinning rate of 8 kHz. Signals marked with asterisks are spinning sidebands.

isotropic motion of 0.2 ns. However, the overall agreement is not as good as for amine-TEMPO. For samples **8** and **7** the lineshape is clearly distinct from the expected for mono-radicals, with additional features at around 335.5 and 337.3 mT. These features are characteristic of biradicals with the spin-exchange Hamiltonian been modulated by conformational transitions, with fast correlation times compared to the EPR time scale [63-71]. The spectra of samples **7, 8** and **9** can be simulated with good agreement by assuming a simplified model, which considers solely two structural conformations: one characterized by $|J| >> |A|$, and another with $|J| << |A|$, where J is the electron-electron spin exchange constant and A is the electron-^{14}N hyperfine coupling parameter. In the first scenario, a coupled spin-1 system interacts with two ^{14}N nuclei, while in the latter, two distinct spin-1/2 systems each interact with a single ^{14}N nucleus. Lineshape variations as a function of the conformational exchange rate k are presented in ESI Figure S25. For samples **7, 8** and **9** the best-fits yields k values of 200, 130 and 20 MHz, respectively. The larger value of k for sample **7** is an indication of the higher probability of coupling between the electron spin pairs, in agreement with the closer proximity between radical species, validating the proposed structure (see Fig. 2). Such correlation between the exchange rate k and inter-radical distances has been documented by Komaguchi et al. [63] for biradicals of two TEMPOs bridged with $–(SiMe_2)_n–$ ($n = 1 – 4$). By changing the length of the $(SiMe_2)_n$ chains they found that shorter lengths correlate with higher exchange rates.

The EPR spectra measured at 100 K for samples **7** – **9** (ESI Figure S26) are consistent with the rigidity of these radicals at low temperatures, as suggested by MD simulations. The spectrum obtained for sample **7** is representative for a nitroxide biradical with non-negligible magnetic electron-electron spin interactions, in agreement with the discussion above. The spectral lineshape for this sample is characteristic for a biradical with electron-electron dipole and exchange coupling interactions.

Proof of spin label applicability for DNP enhanced solid-state NMR

^{1}H MAS and ^{1}H→^{13}C CP MAS spectra for the peptide based biradicals **7, 8** and **9** have been recorded to inspect the efficiency of the synthesized building-blocks for DNP applications. Each peptide radical is dissolved in a glycerol-d_8/D_2O/H_2O (60/30/10), the typical glass forming biotolerant matrix for DNP experiments of biosolids, with a concentration of 15 mM. DNP experiments of the frozen solution have been performed for all three peptide radicals (for details see experimental section). Enhancement factors are obtained by comparison of the spectra measured with and without microwave irradiation employing the same acquisition parameters. Fig. 4 compares the DNP enhanced and, as reference, the thermally polarized ^{1}H MAS NMR and the ^{1}H→^{13}C CP MAS spectra obtained with the radicals **7, 8** and **9**. The ^{1}H MAS spectra are dominated by the signal of frozen water. In the ^{1}H→^{13}C CP MAS

spectra the signal of the peptide is quenched due to the small distance of the nuclei to the radical. The peaks at 60 ppm and 70 ppm are assigned to the carbons in glycerol present in the matrix. The enhancements obtained for glycerol in ^{1}H MAS NMR and $^{1}H\rightarrow^{13}C$ CP MAS of each individual biradical are similar (see ESI Table S1), which indicates a homogeneous distribution of the radicals in frozen solution. For radical **7** (Fig. 4a,b) the largest enhancement of $\varepsilon=45\pm3$ is obtained, which is significantly higher compared to the enhancement for the mono-radical labeled peptides for which only a value of 14 was reached and exceeds even the enhancement of the building block with $\varepsilon=25$ reported previously [40]. For radicals **8** (Fig. 4c,d) and **9** (Fig. 4e,f) enhancement factors of $\varepsilon=29\pm2$ and $\varepsilon=35\pm2$, respectively, are observed. The slightly higher enhancement for radical **7** compared to the other ones most probably refers to the stronger magnetic spin-spin interactions between the electron spins of this peptide radical compared to **8** and **9**. This conclusion is concise with the EPR result discussed above, where stronger electron spin-spin interactions were verified for **7**.

It has to be mentioned that for all investigated peptide radicals the ^{1}H build-up times (see ESI Figures S21-S23) are between 2.5 and 4.5 s, which covers the value for the ^{1}H build-up time (~3.5 s) for the standard DNP juice (10 mM AMUPol in glycerol-d_8/D_2O/H_2O (60/30/10)) [21]. Further improvement of obtained enhancements, which is beyond the scope of this work, is feasible by replacement of the methyl groups in the PROXYL moiety by other substituents as it has been demonstrated for a number of nitroxyl containing radicals in the past [19,20,22].

Conclusion

A versatile strategy for synthesizing tailored peptide based biradicals for DNP NMR applications has been presented. The radical labeled Fmoc-hydroxyproline has been synthesized and inserted at three different positions of a collagen inspired artificial peptide sequence via SPPS to obtain three biradical peptides with different geometry and distances between the radical centers. HPLC and MS analysis have shown the successful introduction of the spin label and EPR spectroscopy has confirmed their chemical integrity after synthesis. DNP enhanced solid-state NMR experiments have shown signal enhancement factors of up to 45 in $^{1}H\rightarrow^{13}C$ CP MAS experiments which correspond to time saving factors of > 2000. This value is a significant improvement compared to an enhancement of 14 reached for a peptide including the mono-radical labeled hydroxyproline building block, and demonstrates significant progress in radical design that aims to produce signal enhancements comparable to optimized commercial radicals such as AMUPol ($\varepsilon>100$). This clearly shows the high potential of our peptide based biradicals for application in DNP enhanced solid-state NMR as well as dissolution DNP. As for example, these peptides may be introduced into proteins or inhibitor molecules as low invasive spin-labels where they can act as specific probes to analyze local interactions and structures.

Authors contributions

KH performed the syntheses and basic characterization of the novel biradicals, and wrote the manuscript draft. MVH measured and processed the DNP and EPR data. HH and FA assisted the DNP NMR measurements and proofread the manuscript. FK performed the synthesis of novel radicals. DR did the MD simulations. MB supported the syntheses of the novel radicals. MOJr. performed the simulations of the EPR data. GB supervised the project and proofread the manuscript. TG concepted the manuscript and co-supervised the project.

CRediT authorship contribution statement

Kevin Herr: Writing – original draft, Methodology, Investigation. **Mark V. Höfler:** Investigation. **Henrike Heise:** Supervision. **Fabien Aussenac:** Supervision. **Felix Kornemann:** Investigation. **David Rosenberger:** Investigation. **Martin Brodrecht:** Supervision, Investigation. **Marcos de Oliveira:** Data curation. **Gerd Buntkowsky:** Writing – review & editing, Supervision, Funding acquisition. **Torsten Gutmann:** Writing – review & editing, Funding acquisition, Conceptualization.

Declaration of competing interest

The authors declare that they have no known competing financial interests or personal relationships that could have appeared to influence the work reported in this paper.

Data availability

Data will be made available on request.

Acknowledgements

Financial support by the Deutsche Forschungsgemeinschaft under contract Bu-911/24–3 is gratefully acknowledged. TG and MVH thank the Deutsche Forschungsgemeinschaft under contract GU-1650/3–1 project number 429632542. MOJr thanks the Brazilian funding agencies FAPESP (grants 2022/02974-1 and 2013/07793-6) and CNPq (grants 312802/2023-4 and 405048/2021-1).

Supplementary materials

Supplementary material associated with this article can be found, in the online version, at doi:10.1016/j.jmro.2024.100152.
Information on analytics (NMR, HPLC, MS, EPR) of the synthesized compounds, solid-state DNP data, ^{1}H build-up curves

Appendix

Synthetic protocols and sample characterization

General

All materials were purchased from commercial suppliers (Fisher Scientific, Acros Organics, Merck, ABCR, Alfa Aesar) and used without further purification unless otherwise described. Solvents were purchased in HPLC grade.

Thin Layer Chromatography

Thin layer chromatography was performed using silica gel (SilG/UV 252, plate thickness: 0.25 mm) by Macherey-Nagel GmbH & Co. KG. Visualization was achieved by UV fluorescence and quenching or oxidizing with $KMnO_4$

Synthesis of radical labeled Fmoc-NH—Hyp-OH

Synthesis of O-tert-butyl N,N'-diisopropylcarbamimidate (3)

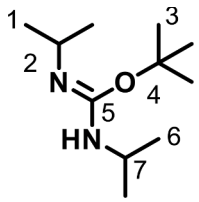

Structure of O-tert-butyl N,N'-diisopropylcarbamimidate **3**.

According to the literature [57], 10.07 mL of N,N'-diisopropylcarbodiimide (65 mmol, 1.0 eq.) and 6.71 mL of tert-butanol (71.5 mmol, 1.1 eq.) were stirred at room temperature under argon atmosphere and finally mixed with 0.065 g Cupper(I)-chloride (0,65 mmol, 0,01 eq). The reaction mixture was stirred overnight at room temperature under argon atmosphere. The progress of the reaction was monitored by thin layer chromatography and also by the change of the color of the mixture from yellow to black. Subsequently, 41.5 mL of DCM (650 mmol, 10 eq.) was added, and the solution was stirred for additional 10 min. ^{1}H and ^{13}C liquid NMR spectra were recorded for reaction control. After completion of the reaction, the protection reaction of the C-terminus of Fmoc-Hydroxyproline **2** with the protection agent **3** was carried out immediately.

^{1}H NMR (300 MHz, $CDCl_3$, 301.2 K): δ (ppm) = 3.64 (sept., 6-H6), 3.13 (2-H, 1H, bs_{cis}, bs_{trans}), 1.46 (s, 9-H3), 1.07,(bs, 6-H1) 1.04 (bs, 6-H6); **^{13}C NMR** (75 MHz, $CDCl_3$, 301.2 K): δ (ppm) = 149.5 (5-C), 78.1 (4-C), 46.1 (2-C), 43.4 (7-C), 28.4 (3-C_3), 24.3 (1-C), 23.8 (6-C).

Synthesis of Fmoc-NH—Hyp(OH)-O^{t}Bu (4)

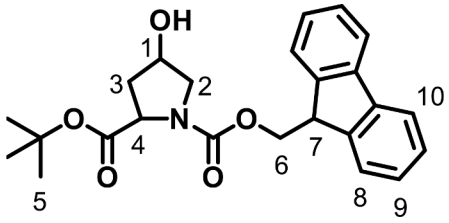

Structure of Fmoc-*NH*—Hyp(OH)-O^{t}Bu **4**.

According to literature [40,72,73] the reaction solution of the first step containing **3** is cooled down to −5 °C. 5.401 g of Fmoc-hydroxyproline **2** (15 mmol, 1 eq.) were dissolved in 75 mL THF and dropwise added to this reaction solution. The mixture turned lime-green. After completion the cooling of the reaction was stopped. The mixture was stirred over night at room temperature and the reaction control was realized by thin layer chromatography. The mixture was filtrated over Celite 545 and solvents removed under reduced pressure. The product was purified by column chromatography (dry load, hexane/ethyl acetate = 1: 2) and solvents removed via rotation evaporator. The product **4** was received as white crystalline solid.

Yield: 1.87 g (26 %); **HPLC$_{254nm}$**: t_R = 5.33 min; **^{1}H NMR** (300 MHz, $CDCl_3$, 301.2 K): δ (ppm) = 7.77–7.60 (9-H, 4H, m), 7.41 (8-H, 2H, ddd, *J* = 6.9 Hz), 7.30 (10-H, 2H, ddd, *J* = 8.6 Hz), 4.53–4.09 (1-H, 3-H, 6-H, 5H, m), 3.76–3.50 (4-H, 7-H, 2H, m), 2.42–2.11 (2-H, 2H, m), 1.45 (5-H, 9H, d, *J* = 10.6 Hz)

Synthesis of Fmoc-NH—Hyp(OOC-PROXYL)-O^{t}Bu (6)

According to literature, [7] 1.87 g of Fmoc-*NH*—Hyp(OH)-OtBu **6** (4.56 mmol, 1.0 eq.) were dissolved in 40 mL of DCM. Afterwards 0.963 g 1-ethyl-3-(3-dimethylaminopropyl)carbodiimide hydrochloride (EDC·HCl) (5.02 mmol, 1.1 eq.), 0.0614 g 4-dimethylaminopyridine (DMAP) (0.502 mmol, 0.11 eq.) and 0.945 g 3-Carboxy-PROXYL **5** (5.02 mmol, 1.1 eq.) were added. The solution turned yellow and was stirred overnight at room temperature. The progress of the reaction was monitored by thin layer chromatography. After completion of the reaction, the reaction mixture was washed with 0.5 M HCl, saturated $NaHCO_3$ solution and brine. The reaction solution was then dried with magnesium sulfate and filtered. The solvent of the filtrate solution was removed using a rotary evaporator. The product **6** was obtained as a yellow crystalline solid.

Yield: 2.6 g (98 %), **HPLC$_{254nm}$**: t_R = 7.22 min, **ESI-MS:** $[M + H]^+$ = 577.3 *m/z* (calc. 577.3 *m/z*)

Synthesis of Fmoc-NH—Hyp(OOC-PROXYL)-OH (1)

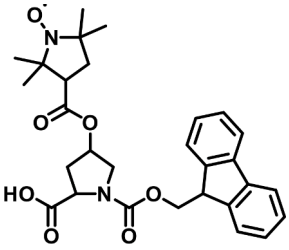

Structure of Fmoc-*NH*—Hyp(OOC-PROXYL)-OH **1**

According to the literature,[7] 2.59 g of Fmoc-NH—Hyp(OOC-PROXYL)-OtBu **6** (4.48 mmol, 1.0 eq.) was dissolved in 30 mL of DCM. The solution was cooled to −5 °C and 33 mL of trifluoroacetic acid (TFA) (402.48 mmol, 89 eq.) were added dropwise. The solution turns black and was stirred at room temperature for 90 min. The solvent was removed under reduced pressure and the remaining black oil was taken up in approximately 50 mL of DCM and washed 3 times each with demineralized water and brine. The organic phase was dried with magnesium sulfate, filtered, and then the solvent removed under reduced pressure. The resulting yellow crude was purified per column chromatography (hexane: ethyl acetate: acetic acid 47.5:47.5:5) yielding **1** as a yellow crystalline solid.

Yield: 1.6 g (68 %); **HPLC$_{254nm}$: t_R** = 4.82 min; **ESI-MS**: $[M + H]^+ = 521.2$ *m/z* (calc. 521.2 *m/z*).

General Procedure of Peptide Synthesis

The syntheses of the peptides were performed according to Amblard et al. [55]

Solvent designations: Both DMF I and DMF II designations refer to the same solvent - dimethylformamide - in different vessels and are used for the washing steps in the synthesis. Here, DMF II is used for the washing steps of coupling. while DMF I is used for Fmoc deprotections. This can reduce contamination with piperidine for DMF II to minimize the risk of negatively affecting the coupling steps.

Resin preactivation of the chlorotrityl resin is implemented in a 10 mL synthesis syringe with a frit bottom. First, the resin is swollen in DMF II for 60 min and then the resin is preactivated with a diisopropylethylamine (DIPEA)/dimethylformamide solution at a ratio of 1 mL/7 mL per gram of resin for 60 min.

Coupling is performed in duplicate and in double excess in each case to achieve maximum high loading. Each Fmoc amino acid is dissolved in 12 mL of DMF II per gram of Fmoc amino acid. To the activated resin, the first Fmoc amino acid is coupled with DIPEA (2.0 eq. based on 1.0 eq. amino acid). Starting with the second coupling, 1-[bis(Dimethylamin)methylen]−1*H*-1,2,3-triazol[4,5-*b*]pyridinium-3-oxid-hexafluorophosphat (HATU) (0.985 eq. based on 1.0 eq. amino acid) is also added. After the reaction solution is drawn onto the syringe containing the resin, the reaction solution is shaken for 30 min. The solution is then removed, and the resin washed four times with DMF II for 1 min each. This coupling is repeated again with the same batch. The resin is then washed 4 times with DMF II for 1 min each. At the end of each coupling, the Fmoc protecting group of the coupled amino acid is cleaved off.

The Fmoc cleavage is used to remove the N-terminal protecting group, adding 20 V % piperidine in dimethyl formamide solution to the resin first for 5 min and then for 15 min. This is followed by washing three times with DMF I and then three times with DMF II for 1 min each. After this step, the next coupling can be performed.

3-carboxy-PROXYL **5** (with DIPEA and HATU) is used as the last coupling. Finally, the resin is washed 6 times with dichloromethane and dried overnight under high vacuum.

Cleavage of the peptide from the resin: 1 mL of cleavage solution (90/5/2.5/2.5 = 95 % trifluoroacetic acid/water/anisole/triisopropylsilane v/v/v/v) is used per 100 mg of resin and the reaction solution is shaken for 3 h. The peptide was precipitated in cold tert-butyl methyl ether, incubated at −20 °C for 30 min, and then washed one time with cold tert-butyl methyl ether and one time with cold dieethyl ether.

The peptides were purified by preparative separations using HPLC analyses. Subsequently, the solvent was removed by lyophilization.

Synthesis of Peptide based Bi-Radicals

Synthesis of PROXYL-Hyp(PROXYL)-Pro-Hyp-Ser-Hyp-Lys-Gly (7)

The synthesis was carried out according to the general procedure of peptide synthesis, and the weights of the individual couplings can be taken from Table 1. Amino acids were coupled to 0.102 g chlorotrityl resin (1.46 mmol/g, 1 eq.) in the order indicated.

37 mg of the crude product **7** was isolated and subsequently purified by preparative HPLC analysis. Here, the separation method had a flow rate of 9 mL/min and a gradient of 0 % to 50 % eluent A in 60 min.

3 mg of the peptide **7** was isolated as a white solid with a purity of > 99 %.

Yield: 1.5 mg (16 %); **HPLC:** t_R = 10.70 min; **EI-MS**: $[M]75^+ = 1075.5$ *m/z* (simulated 1075.5 *m/z*).

Table 1
List of the weights of the individual agents for the synthesis of 7.

Coupling Step	Amino Acid	Equivalents	mMol	Weights [g]
1	Fmoc-Gly-OH	2	0.298	0.089
2	Fmoc-Lys(Boc)-OH	2	0.298	0.14
3	Fmoc-NH-L-Hyp(tBu)-OH	2	0.298	0.122
4	Fmoc-NH-L-Ser(tBu)-OH	2	0.298	0.114
5	Fmoc-NH-L-Hyp(PROXYL)-OH (**1**)	2	0.298	0.155
6	Fmoc-Pro-OH•H_2O	2	0.298	0.106
7	Fmoc-NH-L-Hyp-OH	2	0.298	0.122
8	3-Carboxy-PROXYL (**5**)	2	0.298	0.056

Synthesis of PROXYL-Hyp-Pro-Hyp(PROXYL)-Ser-Hyp-Lys-Gly (8)

The synthesis was carried out according to the general procedure of peptide synthesis, and the weights of the individual couplings can be taken from Table 2. Amino acids were coupled to 0.102 g chlorotrityl resin (1.46 mmol/g, 1 eq.) in the order indicated.

43 mg of crude product **8** could be isolated and subsequently purified by preparative HPLC analysis. Here, the separation method had a flow rate of 9 mL/min and a gradient of 0 % to 50 % eluent A in 60 min.

The peptide **8** obtained could be isolated at 8 mg as a white solid with a purity of > 99 %.

HPLC: t_R = 20.4 min; **ESI-MS**: $[M + H]^+ = 1063.6$ *m/z* (simulated 1063.6 *m/z*); $[M + 2H]^{2+} = 532.8$ *m/z* (simulated 532.8 *m/z*); $[M + 4H]^{3+}$ =

355.9 *m/z* (simulated 355.9 *m/z*)

Table 2
List of weights of the individual coupling agents for the synthesis of 8.

Coupling step	Amino Acid	Equivalents	mMol	Weights [g]
1	Fmoc-Gly-OH	2	0.298	0.089
2	Fmoc-Lys(Boc)-OH	2	0.298	0.14
3	Fmoc-NH-L-Hyp(tBu)-OH	2	0.298	0.122
4	Fmoc-NH-L-Ser(tBu)-OH	2	0.298	0.114
5	Fmoc-NH-L-Hyp(PROXYL)-OH (**1**)	2	0.298	0.155
6	Fmoc-Pro-OH•H_2O	2	0.298	0.106
7	Fmoc-NH-L-Hyp-OH	2	0.298	0.122
8	3-Carboxy-PROXYL (**5**)	2	0.298	0.056

Synthesis of PROXYL-Hyp-Pro-Hyp-Ser-Hyp(PROXYL)-Lys-Gly (9)

The synthesis was carried out according to the general procedure of peptide synthesis, and the weights of the individual couplings can be taken from Table 3. Amino acids were coupled to 0.102 g chlorotrityl resin (1.46 mmol/g, 1 eq.) in the order indicated.

28 mg of the crude product **9** was isolated and subsequently purified by preparative HPLC analysis. Here, the separation method had a flow rate of 9 mL/min and a gradient of 0 % to 50 % eluent A in 60 min.

7 mg of the peptide **9** was isolated as a white solid with a purity of $>$ 99 %.

HPLC: $t_R = 20.10$ min; **ESI-MS**: $[M+H]^+ = 1063.6$ *m/z* (calculated 1063.6 *m/z*); $[M+2H]^{2+} = 532.8$ *m/z* (calculated 532.8 *m/z*); $[M+4H]^{3+} = 355.9$ *m/z* (calculated 355.9 *m/z*)

Table 3
List of weights of the individual coupling agents for the synthesis of 9.

Coupling step	Amino Acid	Equivalent	mMol	Weights [g]
1	Fmoc-Gly-OH	2	0.298	0.089
2	Fmoc-Lys(Boc)-OH	2	0.298	0.14
3	Fmoc-NH-L-Hyp(PROXYL)-OH **1**	2	0.298	0.155
4	Fmoc-NH-L-Ser(tBu)-OH	2	0.298	0.114
5	Fmoc-NH-L-Hyp(tBu)-OH	2	0.298	0.122
6	Fmoc-Pro-OH•H_2O	2	0.298	0.106
7	Fmoc-NH-L-Hyp-OH	2	0.298	0.122
8	3-Carboxy-PROXYL **5**	2	0.298	0.056

Characterization

Liquid NMR

NMR measurements have been conducted using a Bruker 300 MHz Avance III NMR spectrometer or a Bruker 300 MHz Avance II NMR spectrometer (^{1}H-NMR 300.16 MHz, ^{13}C NMR 125.78 MHz) at the service department of the TU Darmstadt. The chemical shifts are given in ppm. As internal standard the chemical shift of the solvent peak was used.

Reverse phase high-performance liquid chromatography (RP-HPLC)

Reverse phase high-performance liquid chromatography (RP-HPLC) for analytical purposes was conducted using a Waters HPLC setup consisting of a Waters Alliance e2695 equipped with a Waters 2998 PDA detector. The detection wavelength was chosen depending on the analyte between 214, 254, 280 and 301 nm. The eluent system for the HPLC system comprised eluent A (0.1 % aq. TFA) and eluent B (99.9 % acetonitrile containing 0.1 % TFA). Unless otherwise specified analytical HPLC runs were conducted at a flow rate of 2 ml/min with an eluent gradient from 20 % to 80 % of eluent B in eluent A over 10 min. For building-block analysis a RP 18 HP column from CS Chromatographie (3 µm, 120 Å) was used. For peptide analysis a Nucleosil 100–5C18 column from Macerey-Nagel (5 µm, 100 Å) was used. Preparative purification of the peptides was performed on a Knauer Multokrom RP18 column 20 $\times$ 250 mm (5 µm, 100 Å) employing a flow rate of 9 mL/min and an acetonitril gradient from 0 % to 50 % without TFA in water over the course of 60 min.

Electrospray mass spectrometry (ESI-MS)

Electron spray ionization (ESI) mass spectra were recorded with a Bruker Esquire-LC mass spectrometer at the service department of the TU Darmstadt.

References

[1] V.S. Bajaj, M.L. Mak-Jurkauskas, M. Belenky, J. Herzfeld, R.G. Griffin, DNP enhanced frequency-selective TEDOR experiments in bacteriorhodopsin, J. Magn. Reson. 202 (2010) 9–13, https://doi.org/10.1016/j.jmr.2009.09.005.

[2] G.T. Debelouchina, M.J. Bayro, A.W. Fitzpatrick, V. Ladizhansky, M.T. Colvin, M. A. Caporini, C.P. Jaroniec, V.S. Bajaj, M. Rosay, C.E. MacPhee, et al., Higher Order Amyloid Fibril Structure by MAS NMR and DNP Spectroscopy, J. Am. Chem. Soc. 135 (2013) 19237–19247, https://doi.org/10.1021/ja409050a.

[3] I. Gelis, V. Vitzthum, N. Dhimole, M.A. Caporini, A. Schedlbauer, D. Carnevale, S. R. Connell, P. Fucini, G. Bodenhausen, Solid-state NMR enhanced by dynamic nuclear polarization as a novel tool for ribosome structural biology, J. Biomol. NMR 56 (2013) 85–93, https://doi.org/10.1007/s10858-013-9721-2.

[4] M. Renault, A. Cukkemane, M. Baldus, Solid-State NMR Spectroscopy on Complex Biomolecules, Angew. Chem. Int. Ed. 49 (2010) 8346–8357, https://doi.org/10.1002/anie.201002823.

[5] A.G. Rankin, J. Trebosc, F. Pourpoint, J.P. Amoureux, O. Lafon, Recent developments in MAS DNP-NMR of materials, Solid State Nucl. Magn. Reson. 101 (2019) 116–143, https://doi.org/10.1016/j.ssnmr.2019.05.009.

[6] T. Biedenbaender, V. Aladin, S. Saeidpour, B. Corzilius, Dynamic Nuclear Polarization for Sensitivity Enhancement in Biomolecular Solid-State NMR, Chem. Rev. 122 (2022) 9738–9794, https://doi.org/10.1021/acs.chemrev.1c00776.

[7] W.Y. Chow, G. de Paepe, S. Hediger, Biomolecular and Biological Applications of Solid-State NMR with Dynamic Nuclear Polarization Enhancement, Chem. Rev. 122 (2022) 9795–9847, https://doi.org/10.1021/acs.chemrev.1c01043.

[8] I.B. Moroz, M. Leskes, Dynamic Nuclear Polarization Solid-State NMR Spectroscopy for Materials Research, Ann. Rev. Mater. Res. 52 (2022) 25–55, https://doi.org/10.1146/annurev-matsci-081720-085634.

[9] Q.Z. Ni, E. Daviso, T.V. Can, E. Markhasin, S.K. Jawla, T.M. Swager, R.J. Temkin, J. Herzfeld, R.G. Griffin, High Frequency Dynamic Nuclear Polarization, Acc. Chem. Res. 46 (2013) 1933–1941, https://doi.org/10.1021/ar300348n.

[10] L. Zhao, A.C. Pinon, L. Emsley, A.J. Rossini, DNP-enhanced solid-state NMR spectroscopy of active pharmaceutical ingredients, Magn. Reson. Chem. 56 (2018) 583–609, https://doi.org/10.1002/mrc.4688.

[11] T. Gutmann, P.B. Groszewicz, G. Buntkowsky, Solid-state NMR of nanocrystals, Annu. Rep. NMR Spec. 97 (2019) 1–82, https://doi.org/10.1016/bs.arnmr.2018.12.001.

[12] M. Werner, A. Heil, N. Rothermel, H. Breitzke, P.B. Groszewicz, A.S. Thankamony, T. Gutmann, G. Buntkowsky, Synthesis and solid state NMR characterization of novel peptide/silica hybrid materials, Solid State Nucl. Magn. Reson. 72 (2015) 73–78, https://doi.org/10.1016/j.ssnmr.2015.09.008.

[13] M. Brodrecht, B. Kumari, A.S. Thankamony, Sofia Lilly, H. Breitzke, T. Gutmann, G. Buntkowsky, Structural Insights into Peptides Bound to the Surface of Silica Nanopores, Chem. Eur. J. 25 (2019) 5214–5221, https://doi.org/10.1002/chem.201805480.

[14] D. Gauto, O. Dakhlaoui, I. Marin-Montesinos, S. Hediger, G. de Paëpe, Targeted DNP for biomolecular solid-state NMR, Chem. Sci. 12 (2021) 6223–6237, https://doi.org/10.1039/d0sc06959k.

[15] U. Akbey, W.T. Franks, A. Linden, M. Orwick-Rydmark, S. Lange, H. Oschkinat, Dynamic nuclear polarization enhanced NMR in the solid-state. Hyperpolarization Methods in NMR Spectroscopy, Springer, 2013, pp. 181–228.

[16] A.S. Lilly Thankamony, J.J. Wittmann, M. Kaushik, B. Corzilius, Dynamic nuclear polarization for sensitivity enhancement in modern solid-state NMR, Prog. Nucl. Magn. Reson. Spectrosc. 102-103 (2017) 120–195, https://doi.org/10.1016/j.pnmrs.2017.06.002.

[17] G. Menzildjian, J. Schlagnitweit, G. Casano, O. Ouari, D. Gajan, A. Lesage, Polarizing agents for efficient high field DNP solid-state NMR spectroscopy under magic-angle spinning: from design principles to formulation strategies, Chem. Sci. 14 (2023) 6120–6148, https://doi.org/10.1039/D3SC01079A.

[18] W.-C. Liao, T.-C. Ong, D. Gajan, F. Bernada, C. Sauvée, M. Yulikov, M. Pucino, R. Schowner, M. Schwarzwälder, M.R. Buchmeiser, et al., Dendritic polarizing agents for DNP SENS, Chem. Sci. 8 (2017) 416–422, https://doi.org/10.1039/C6SC03139K.

[19] R. Harrabi, T. Halbritter, F. Aussenac, O. Dakhlaoui, J. van Tol, K.K. Damodaran, D. Lee, S. Paul, S. Hediger, F. Mentink-Vigier, et al., Highly Efficient Polarizing Agents for MAS-DNP of Proton-Dense Molecular Solids, Angew. Chem. Int. Ed. 61 (2022) e202114103, https://doi.org/10.1002/anie.202114103.

[20] F. Mentink-Vigier, I. Marin-Montesinos, A.P. Jagtap, T. Halbritter, J. van Tol, S. Hediger, D. Lee, S.T. Sigurdsson, G. de Paepe, Computationally Assisted Design of Polarizing Agents for Dynamic Nuclear Polarization Enhanced NMR: The AsymPol Family, J. Am. Chem. Soc. 140 (2018) 11013–11019, https://doi.org/10.1021/jacs.8b04911.

[21] C. Sauvée, M. Rosay, G. Casano, F. Aussenac, R.T. Weber, O. Ouari, P. Tordo, Highly Efficient, Water-Soluble Polarizing Agents for Dynamic Nuclear Polarization at High Frequency, Angew. Chem. Int. Ed. 52 (2013) 10858–10861, https://doi.org/10.1002/anie.201304657.

[22] A. Zagdoun, G. Casano, O. Ouari, M. Schwarzwälder, A.J. Rossini, F. Aussenac, M. Yulikov, G. Jeschke, C. Copéret, A. Lesage, et al., Large Molecular Weight Nitroxide Biradicals Providing Efficient Dynamic Nuclear Polarization at Temperatures up to 200 K, Journal of the American Chemical Society 135 (2013) 12790–12797, https://doi.org/10.1021/ja405813t.

[23] S. Bothe, J. Nowag, V. Klimavicius, M. Hoffmann, T.I. Troitskaya, E.V. Amosov, V. M. Tormyshev, I. Kirilyuk, A. Taratayko, A. Kuzhelev, et al., Novel Biradicals for Direct Excitation Highfield Dynamic Nuclear Polarization, J. Phys. Chem. C 122 (2018) 11422–11432, https://doi.org/10.1021/acs.jpcc.8b02570.

[24] W.X. Zhai, A.L. Paioni, X.Y. Cai, S. Narasimhan, J. Medeiros-Silva, W.X. Zhang, A. Rockenbauer, M. Weingarth, Y.G. Song, M. Baldus, et al., Postmodification via Thiol-Click Chemistry Yields Hydrophilic Trityl-Nitroxide Biradicals for Biomolecular High-Field Dynamic Nuclear Polarization, J. Phys. Chem. B 124 (2020) 9047–9060, https://doi.org/10.1021/acs.jpcb.0c08321.

[25] K.R. Thurber, T.N. Le, V. Changcoco, D.J. Brook, Verdazyl-ribose: A new radical for solid-state dynamic nuclear polarization at high magnetic field, J. Magn. Reson. 289 (2018) 122–131, https://doi.org/10.1016/j.jmr.2018.02.016.

[26] A. Lund, G. Casano, G. Menzildjian, M. Kaushik, G. Stevanato, M. Yulikov, R. Jabbour, D. Wisser, M. Renom-Carrasco, C. Thieuleux, et al., TinyPols: a family of water-soluble binitroxides tailored for dynamic nuclear polarization enhanced NMR spectroscopy at 18.8 and 21.1 T, Chem. Sci. 11 (2020) 2810–2818, https://doi.org/10.1039/c9sc05384k.

[27] A.P. Jagtap, M.A. Geiger, D. Stoppler, M. Orwick-Rydmark, H. Oschkinat, S. T. Sigurdsson, bcTol: a highly water-soluble biradical for efficient dynamic nuclear polarization of biomolecules, Chem. Commun. 52 (2016) 7020–7023, https://doi.org/10.1039/c6cc01813k.

[28] N.B. Asanbaeva, S.A. Dobrynin, Da Morozov, N. Haro-Mares, T. Gutmann, G. Buntkowsky, E.G. Bagryanskaya, An EPR Study on Highly Stable Nitroxyl-Nitroxyl Biradicals for Dynamic Nuclear Polarization Applications at High Magnetic Fields, Molecules 28 (2023), https://doi.org/10.3390/molecules28041926.

[29] A. Radaelli, Hikari A., I Yoshihara, H. Nonaka, S. Sando, J.H. Ardenkjaer-Larsen, R. Gruetter, A. Capozzi, 13C Dynamic Nuclear Polarization using SA-BDPA at 6.7 T and 1.1 K: Coexistence of Pure Thermal Mixing and Well-Resolved Solid Effect, J. Phys. Chem. Lett. 11 (2020) 6873–6879, https://doi.org/10.1021/acs.jpclett.0c01473.

[30] M.-A. Geiger, A.P. Jagtap, M. Kaushik, H. Sun, D. Stöppler, S.T. Sigurdsson, B. Corzilius, H. Oschkinat, Efficiency of Water-Soluble Nitroxide Biradicals for Dynamic Nuclear Polarization in Rotating Solids at 9.4 T: bcTol-M and cyolyl-TOTAPOL as New Polarizing Agents, Chem. Eur. J. 24 (2018) 13485–13494.

[31] R. Yao, D. Beriashvili, W. Zhang, S. Li, A. Safeer, A. Gurinov, A. Rockenbauer, Y. Yang, Y. Song, M. Baldus, et al., Highly bioresistant, hydrophilic and rigidly linked trityl-nitroxide biradicals for cellular high-field dynamic nuclear polarization, Chem. Sci. 13 (2022) 14157–14164, https://doi.org/10.1039/D2SC04668G.

[32] J.F. Mao, D. Akhmetzyanov, O. Ouari, V. Denysenkov, B. Corzilius, J. Plackmeyer, P. Tordo, T.F. Prisner, C. Glaubitz, Host-Guest Complexes as Water-Soluble High-Performance DNP Polarizing Agents, J. Am. Chem. Soc. 135 (2013) 19275–19281, https://doi.org/10.1021/ja409840y.

[33] M. Lelli, A.J. Rossini, G. Casano, O. Ouari, P. Tordo, A. Lesage, L. Emsley, Hydrophobic radicals embedded in neutral surfactants for dynamic nuclear polarization of aqueous environments at 9.4 Tesla, Chem. Commun. 50 (2014) 10198–10201, https://doi.org/10.1039/C4CC02152E.

[34] D.J. Kubicki, G. Casano, M. Schwarzwalder, S. Abel, C. Sauvee, K. Ganesan, M. Yulikov, A.J. Rossini, G. Jeschke, C. Coperet, et al., Rational design of dinitroxide biradicals for efficient cross-effect dynamic nuclear polarization, Chem. Sci. 7 (2016) 550–558, https://doi.org/10.1039/c5sc02921j.

[35] G. Casano, H. Karoui, O. Ouari, Polarizing Agents: Evolution and Outlook in Free Radical Development for DNP, Emagres 7 (2018) 195–207, https://doi.org/10.1002/9780470034590.emrstm1547.

[36] F.A. Perras, A. Sadow, M. Pruski, In Silico Design of DNP Polarizing Agents: Can Current Dinitroxides Be Improved? ChemPhysChem 18 (2017) 2279–2287, https://doi.org/10.1002/cphc.201700299.

[37] G. Stevanato, G. Casano, D.J. Kubicki, Y. Rao, Le Hofer, G. Menzildjian, H. Karoui, D. Siri, M. Cordova, M. Yulikov, et al., Open and Closed Radicals: Local Geometry around Unpaired Electrons Governs Magic-Angle Spinning Dynamic Nuclear Polarization Performance, J. Am. Chem. Soc. 142 (2020) 16587–16599, https://doi.org/10.1021/jacs.0c04911.

[38] M.-A. Sani, S. Zhu, V. Hofferek, F. Separovic, Nitroxide spin–labeled peptides for DNP-NMR in-cell studies, The FASEB Journal 33 (2019) 11021–11027, https://doi.org/10.1096/fj.201900931R.

[39] S. Zhu, E. Kachooei, J.R. Harmer, L.J. Brown, F. Separovic, M.-A. Sani, TOAC spin-labeled peptides tailored for DNP-NMR studies in lipid membrane environments, Biophys. J. 120 (2021) 4501–4511, https://doi.org/10.1016/j.bpj.2021.08.040.

[40] M. Brodrecht, K. Herr, S. Bothe, M. de Oliveira Jr, T. Gutmann, G. Buntkowsky, Efficient Building Blocks for Solid-Phase Peptide Synthesis of Spin Labeled Peptides for Electron Paramagnetic Resonance and Dynamic Nuclear Polarization Applications, ChemPhysChem 20 (2019) 1475–1487.

[41] S. Stoll, A. Schweiger, EasySpin, a comprehensive software package for spectral simulation and analysis in EPR, J. Magn. Reson. 178 (2006) 42–55, https://doi.org/10.1016/j.jmr.2005.08.013.

[42] M. Zalibera, A.S. Jalilov, S. Stoll, I.A. Guzei, G. Gescheidt, S.F. Nelsen, Monotrimethylene-Bridged Bis-p-phenylenediamine Radical Cations and Dications: Spin States, Conformations, and Dynamics, J. Phys. Chem. A 117 (2013) 1439–1448, https://doi.org/10.1021/jp3104358.

[43] D. Cory, W. Ritchey, Suppression of signals from the probe in bloch decay spectra, J. Magn. Reson. 80 (1988) 128–132, https://doi.org/10.1016/0022-2364(88)90064-9.

[44] B.M. Fung, A.K. Khitrin, K. Ermolaev, An improved broadband decoupling sequence for liquid crystals and solids, J. Magn. Reson. 142 (2000) 97–101, https://doi.org/10.1006/jmre.1999.1896.

[45] J.C. Jackson, J.T. Hammill, R.A. Mehl, Site-Specific Incorporation of a 19F-Amino Acid into Proteins as an NMR Probe for Characterizing Protein Structure and Reactivity, J. Am. Chem. Soc. 129 (2007) 1160–1166, https://doi.org/10.1021/ja064661t.

[46] A.J. Link, M.L. Mock, D.A. Tirrell, Non-canonical amino acids in protein engineering, Curr. Opin. Biotechnol. 14 (2003) 603–609, https://doi.org/10.1016/j.copbio.2003.10.011.

[47] Y.-W. Wu, R.S. Goody, Probing protein function by chemical modification, J. Pept. Sci. 16 (2010) 514–523, https://doi.org/10.1002/psc.1287.

[48] F.-L. Yeh, L. Tung, T.-H. Chang, Detection of Protein–Protein Interaction Within an RNA–Protein Complex Via Unnatural-Amino-Acid-Mediated Photochemical Crosslinking, in: R.-J. Lin (Ed.), RNA-Protein Complexes and Interactions: Methods and Protocols, Springer, New York, 2016, pp. 175–189.

[49] M.M. Zegota, T. Wang, C. Seidler, D.Y. Wah Ng, S.L. Kuan, T. Weil, Tag and Modify" Protein Conjugation with Dynamic Covalent Chemistry, Bioconjugate Chem 29 (2018) 2665–2670, https://doi.org/10.1021/acs.bioconjchem.8b00358.

[50] E. Zurlo, I. Gorroño Bikandi, N.J. Meeuwenoord, D.V. Filippov, M. Huber, Tracking amyloid oligomerization with monomer resolution using a 13-amino acid peptide with a backbone-fixed spin label, Phys. Chem. Chem. Phys. 21 (2019) 25187–25195, https://doi.org/10.1039/C9CP01060B.
[51] H. Sahoo, Fluorescent labeling techniques in biomolecules: a flashback, RSC Adv 2 (2012) 7017–7029, https://doi.org/10.1039/C2RA20389H.
[52] H. Wang, H. Gao, N. Guo, G. Niu, Y. Ma, D.O. Kiesewetter, X. Chen, Site-Specific Labeling of scVEGF with Fluorine-18 for Positron Emission Tomography Imaging, Theranostics 2 (2012) 607–617, https://doi.org/10.7150/thno.4611.
[53] J.M. Chalker, G.J.L. Bernardes, B.G. Davis, A "Tag-and-Modify" Approach to Site-Selective Protein Modification, Acc. Chem. Res. 44 (2011) 730–741, https://doi.org/10.1021/ar200056q.
[54] R.B. Merrifield, Solid phase peptide synthesis. I. The synthesis of a tetrapeptide, J. Am. Chem. Soc. 85 (1963) 2149–2154, https://doi.org/10.1021/ja00897a025.
[55] M. Amblard, J.-A. Fehrentz, J. Martinez, G. Subra, Methods and protocols of modern solid phase peptide synthesis, Mol. Biotechnol. 33 (2006) 239–254.
[56] B. Neises, W. Steglich, Simple Method for the Esterification of Carboxylic Acids, Angew. Chem. Int. Ed. 17 (1978) 522–524, https://doi.org/10.1002/anie.197805221.
[57] E. Huerta, B. van Genabeek, P.J.M. Stals, E.W. Meijer, A.R.A. Palmans, A Modular Approach to Introduce Function into Single-Chain Polymeric Nanoparticles, Macromol. Rapid Commun. 35 (2014) 1320–1325, https://doi.org/10.1002/marc.201400213.
[58] M.K. Kiesewetter, B. Corzilius, A.A. Smith, R.G. Griffin, T.M. Swager, Dynamic nuclear polarization with a water-soluble rigid biradical, J. Am. Chem. Soc. 134 (2012) 4537–4540, https://doi.org/10.1021/ja212054e.
[59] S. Xu, M. Gu, K. Wu, G. Li, Unraveling the Role of Hydroxyproline in Maintaining the Thermal Stability of the Collagen Triple Helix Structure Using Simulation, J. Phys. Chem. B 123 (2019) 7754–7763, https://doi.org/10.1021/acs.jpcb.9b05006.
[60] A. Ghanaeian, R. Soheilifard, Mechanical elasticity of proline-rich and hydroxyproline-rich collagen-like triple-helices studied using steered molecular dynamics, J. Mech. Behav. Biomed. Mater. 86 (2018) 105–112, https://doi.org/10.1016/j.jmbbm.2018.06.021.
[61] P. Bjelkmar, P. Larsson, M.A. Cuendet, B. Hess, E. Lindahl, Implementation of the CHARMM Force Field in GROMACS: Analysis of Protein Stability Effects from Correction Maps, Virtual Interaction Sites, and Water Models, J. Chem. Theory Comput. 6 (2010) 459–466, https://doi.org/10.1021/ct900549r.
[62] M.G. Santangelo, M. Levantino, A. Cupane, G. Jeschke, Solvation of a Probe Molecule by Fluid Supercooled Water in a Hydrogel at 200 K, J. Phys. Chem. B 112 (2008) 15546–15553, https://doi.org/10.1021/jp805131j.
[63] K. Komaguchi, T. Iida, Y. Goh, J. Ohshita, A. Kunai, M. Shiotani, An ESR study of dynamic biradicals of two TEMPOs bridged with –(SiMe2)n– (n=1–4) in liquid solution, Chem. Phys. Lett. 387 (2004) 327–331, https://doi.org/10.1016/j.cplett.2004.02.010.
[64] S.S. Eaton, L.B. Woodcock, G.R. Eaton, Continuous wave electron paramagnetic resonance of nitroxide biradicals in fluid solution, Concepts Magn. Reson. Part A 47A (2018) e21426, https://doi.org/10.1002/cmr.a.21426.
[65] S. Sankarapandi, G.V. Chandramouli, C. Daul, P.T. Manoharan, Fast Computation of Dynamic EPR-Spectra of Biradicals, J. Magn. Reson., Ser. A 103 (1993) 163–170, https://doi.org/10.1006/jmra.1993.1147.
[66] J. Soetbeer, P. Gast, J.J. Walish, Y.C. Zhao, C. George, C. Yang, T.M. Swager, R. G. Griffin, G. Mathies, Conformation of bis-nitroxide polarizing agents by multi-frequency EPR spectroscopy, Phys. Chem. Chem. Phys. 20 (2018) 25506–25517, https://doi.org/10.1039/c8cp05236k.
[67] M.S. Palha, E.A. Legenzov, N.D. Dirda, G.M. Rosen, J.P. Kao, New Disulfide-Linked Dinitroxides and the Kinetics of Their Reaction with Glutathione, Appl. Magn. Reson. 52 (2021) 945–955, https://doi.org/10.1007/s00723-021-01332-3.
[68] J.P. Kao, W. Moore, L.B. Woodcock, N.D. Dirda, E.A. Legenzov, S.S. Eaton, G. R. Eaton, Nitroxide Diradical EPR Lineshapes and Spin Relaxation, Appl. Magn. Reson. 53 (2022) 221–232, https://doi.org/10.1007/s00723-021-01372-9.
[69] A.I. Kokorin, V.N. Khrustalev, E.N. Golubeva, The Structure and EPR Behavior of Short Nitroxide Biradicals Containing Sulfur Atom in the Bridge, Appl. Magn. Reson. 45 (2014) 397–409, https://doi.org/10.1007/s00723-014-0528-4.
[70] D.A. Shultz, A.K. Boal, H. Lee, G.T. Farmer, Structure-property relationships in trimethylenemethane-type biradicals. 2. Synthesis and EPR spectral characterization of dinitroxide biradicals, J. Org. Chem. 64 (1999) 4386–4396, https://doi.org/10.1021/jo990061j.
[71] D.C. Oniciu, K. Matsuda, H. Iwamura, Synthesis and EPR characterisation of triphenylmethane derivatives carrying N-tert-butyl nitroxide radical moieties: Use of the diradical as a ligand for a complex with Mn-II(hfac)(2), J. Chem. Soc., Perkin Trans. 2 (1996) 907–913, https://doi.org/10.1039/p29960000907.
[72] P.J. Knerr, W.A. van der Donk, Chemical synthesis and biological activity of analogues of the lantibiotic epilancin 15X, J. Am. Chem. Soc. 134 (2012) 7648–7651.
[73] M. Heuckendorff, H.H. Jensen, Removal of some common glycosylation by-products during reaction work-up, Carbohydr. Res. 439 (2017) 50–56, https://doi.org/10.1016/j.carres.2016.12.007.